Performance evaluation of a CyberKnife® G4 image-guided robotic stereotactic radiosurgery system

Christos Antypas[1,2] **and Evaggelos Pantelis**[1]

[1] Medical Physics Department, Iatropolis, Magnitiki Tomografia, Clinic and Diagnostic Center, Ethnikis Antistaseos 54-56, 15231 Athens, Greece
[2] Department of Radiology, Aretaieion Hospital, University of Athens, Vas Sophias 56, 11528 Athens, Greece

E-mail: cantypas@med.uoa.gr

Abstract

The aim of the current work was to present the performance evaluation procedures implemented at our department for the commissioning of a G4 CyberKnife system. This system consists of a robotic manipulator, a target-locating system and a lightweight 6-MV linac. Individual quality assurance procedures were performed for each of the CyberKnife subsystems. The system was checked for the mechanical accuracy of its robotic manipulator. The performance of the target-locating system was evaluated in terms of mechanical accuracy of both cameras' alignment and quality assurance tests of the x-ray generators and the flat-panel detectors. The traditional linac 6-MV beam characteristics and beam output parameters were also measured. Results revealed a manipulator mechanical mean accuracy of $\sim$0.1 mm, with individual maximum position uncertainties less than 0.25 mm. The target-locating system mechanical accuracy was found within the acceptance limits. For the most clinically used parameters in the CyberKnife practice, e.g. 100–120 kV and 50–200 ms, kV and exposure time accuracy error were measured as less than 2%, while the precision error of the kV was determined as less than 1%. The acquired images of the ETR grid pattern revealed no geometrical distortion while the critical frequency f_{50} values for cameras A and B were calculated as 1.5 lp mm^{-1} and 1.4 lp mm^{-1}, respectively. Dose placement measurements were performed in a head and neck phantom. Results revealed sub-millimeter beam delivery precision whereas the total clinical accuracy of the system was measured equal to 0.44 ± 0.12 mm, 0.29 ± 0.10 mm and 0.53 ± 0.16 mm for the skull, fiducial and Xsight spine tracking methods, respectively. The results of this work certify the G4 CyberKnife SRS system capable of delivering high dose distributions with sub-millimeter accuracy and precision to intracranial and extracranial lesions. Moreover, total clinical accuracy of the investigated G4 system was found to be improved for the skull and fiducial tracking methods

and was comparable for Xsight spine tracking method compared with the earlier generation of the instrument.

1. Introduction

In stereotactic radiosurgery and stereotactic radiotherapy, single or multiple fractions of a high radiation dose are delivered to a well-defined small target. SRS has become an important treatment modality in the management of a wide variety of intracranial and extracranial lesions, offering the possibility for a significant reduction of dose to critical healthy tissues with significant benefit to patients (Wurm and Okunieff 2006, Kavanagh and Timmerman 2006, Mehta *et al* 2005, Tsao *et al* 2005, Nishizaki *et al* 2006, Romanelli *et al* 2006a, 2006b, Casamassima *et al* 2006, Strassmann *et al* 2006, Wu *et al* 2006). The CyberKnife® (CK) SRS system (Accuray Incorporated, Sunnyvale, California, USA) is a frameless radio surgery device that combines image guidance with robotic technology aiming at the delivery of highly conformal dose distributions to intracranial and extracranial lesions with a standard uncertainty of less than 1 mm (Murphy and Cox 1996, Adler *et al* 1999, Kuo *et al* 2003, Chang *et al* 2003, Schweikard *et al* 2004, Romanelli *et al* 2006a, 2006b, Muacevic *et al* 2006).

Four generations of the CyberKnife system have been released and accuracy on clinical procedures of each generation has been studied (generation 1—Murphy and Cox (1996), generation 2—Chang *et al* (2003), generation 3—Yu *et al* (2004a, 2004b)). Furthermore, there are numerous publications on small-field dosimetry and output factor measurements. Various dosimetric means have also been used and investigated for various SRS systems, including Gamma Knife® (Elekta AG, Stockholm, Sweden) and XKnife™ (Integra Radionics, Inc., Burlington, Massachusetts) (Heydarian *et al* 1996, Francescon *et al* 1998, Yu *et al* 2004a, 2004b , Karaiskos *et al* 2005, Pappas *et al* 2005, 2006, Wilcox and Daskalov 2007). However, the literature lacks publications dedicated to the commissioning and quality assurance procedures for acceptance testing of the CyberKnife system. The robotic technology, image guidance based on sophisticated target localization software and the small field dosimetry issues, e.g. detector choice (Pantelis *et al* 2008), that are incorporated into CyberKnife present multiple challenges for physicists who have to perform the commissioning of the system. Considering that CyberKnife is a non-standard system, inevitably, the physicist/user has to follow some vendor's recommended procedures for part of the commissioning.

A generation four (G4) model of the CyberKnife SRS system has been installed in our department. The aim of the current work is to present the performance evaluation procedures we performed for the commissioning of this system and the results obtained. Individual quality control checks for each of the CyberKnife sub-systems were carried out. Namely, mechanical accuracy of the robotic manipulator movements, mechanical alignment of the imaging system, performance of the x-ray tubes and image quality of the detectors were assessed. The dosimetric beam characteristics of the 6-MV beam were also measured. Finally, beam delivery precision and total clinical accuracy of the system, incorporating all individual steps of the treatment procedure, were evaluated.

2. Materials and methods

2.1. Description of the G4 CyberKnife SRS system

In brief, CyberKnife utilizes a six-axis jointed robotic arm (KUKA Roboter GmbH, Germany) to manipulate a compact and lightweight 6-MV linear accelerator (linac). The linac beam

is collimated using 12 circular collimators of 5–60 mm nominal size defined at SAD = 80 cm. The treatment couch of our CyberKnife system is a computer-controlled couch with five degrees of freedom that is able to remotely position the patient. The target localization system consists of two standard kilovoltage x-ray generators and two amorphous silicon flat-panel digital detectors, called hereafter cameras A and B. The target locating system cameras are mounted in orthogonal configuration on the ceiling and in the floor of the treatment room. Images from both cameras are fed into the image-guidance software, which uses an image registration algorithm to track the target, i.e. to calculate translations and rotations of the target throughout the treatment (Fu and Kuduvalli 2008). In our G4 CyberKnife system, three tracking methods are installed and used for image-guided intracranial and extracranial clinical applications. The fiducial tracking method is used for extracranial applications with internal radio opaque markers implanted into the soft tissue surrounding the target (Murphy 2002). The skull tracking method that is designed for intracranial applications is based on rigid body registration of bony landmarks of the patient's head (Fu *et al* 2005). Xsight spine tracking method, designed for spine applications, is based on non-rigid body registration of spinal bony landmarks (Ho *et al* 2007).

An axial CT scan of the target region is used for the treatment planning. The treatment procedure is based on the image guidance principle. Digitally reconstructed radiographs (DRRs) are created for the respective Target Locating System cameras' geometric configuration. Initially and during the treatment, a pair of live x-ray images is acquired and compared with the patient's treatment planning DRRs. Translations and rotations computed by the appropriate tracking method algorithm are fed into the robot manipulator prior to the delivery of each beam (Fu and Kuduvalli 2008). The system is able to track and realign the linac for translations and rotations of the target up to 10 mm and 3°, respectively. If the displacement of the target exceeds these limits, the operation is paused for remote realignment of the patient using the couch.

Compared with previous generations, the main distinctions of the G4 CyberKnife model are the increased dose rate of the linac beam, up to 600 MU min^{-1} and the new geometry of the Target Locating System detectors, resulting in shorter treatment times and increased robot mobility around the treatment couch.

2.2. Quality control of the CyberKnife subsystems

2.2.1. Manipulator mechanical accuracy. A treatment path consists of a series of nodes the robot manipulator travels from one to the next during a treatment course. Each node is a potential point in space from which the linac beam can be directed toward the target and is represented by a set of Cartesian coordinates of the space around the target (Murphy and Cox 1996). Depending on the clinical application, head or body, the robot travels through treatment paths at different distances from the target that may be 650 mm, 800 mm or 1000 mm. The robot is initially calibrated to direct the linac beam from each node to a specific point in space called 'the imaging center,' which is physically represented by a small crystal situated on top of a floor-mounted post, called isopost, (Murphy and Cox 1996). Mechanical accuracy of the manipulator was evaluated by instructing the robotic arm to pass through all the nodes of a treatment path, determining at each node the linac beam direction over a fine mesh of points surrounding the isopost. The linac beam central axis and pointing direction are represented by a laser beam of 1 mm in diameter. Laser light striking the isopost is directed by an optical fiber to a light sensitive diode. The signal created in the diode is then amplified and monitored. The closer the laser beam strikes the center of the crystal a proportionately larger signal is created inside the diode. The manipulator coordinates that correspond to the

maximum signal created by the crystal are stored and compared with the corresponding values calculated during calibration. Manipulator mechanical accuracy in positioning the linac at each node can then be expressed as a radial displacement error, dr_i, of the node coordinates obtained during the evaluation and calibration procedures:

$$dr_i = \sqrt{dx_i^2 + dy_i^2 + dz_i^2}. \tag{1}$$

The maximum individual radial displacement, dr_{max}, and the mean radial displacement, $\overline{dr}$, of the nodes that make up a treatment path are recorded for each of the available treatment paths.

2.2.2. Target locating system performance evaluation.

Mechanical accuracy of the target locating system cameras' alignment. Mechanical accuracy of the alignment of each camera was evaluated by mounting the isopost on the treatment room floor and imaging its position. The coordinates of the projected crystal should be in the central pixel of both images A and B with a maximum tolerance of ± 1 mm in both image directions.

Target locating system x-ray generators: accuracy and precision of kilovoltage and exposure time settings. Consistency of the target locating system is dependent on the quality of the radiographs recorded by the cameras. In general, the accuracy and precision of kilovoltage (kV_p) indicator and exposure timer should be evaluated at acceptance and checked periodically thereafter (Shepard *et al* 2002). A non-invasive multifunction meter was used to measure kV_p values and exposure times (DIAVOLT UNIVERSAL T43014 PTW, Freiburg, Germany). The multifunction meter was positioned at the imaging center facing the x-ray tube being tested. A set of measurements was taken for each generator using nominal kV values in the range of 70–120 kV and 20 ms–500 ms. Accuracy is defined using the mean deviation of a set of experimental values from the expected nominal value. Precision is defined as a measure of the deviation of each individual experimental value from the mean experimental value. According to specifications and quality assurance protocols for x-ray generators (Rossi *et al* 1985, Shepard *et al* 2002) uncertainty of kV_p measurements must be less than 5% (Rossi *et al* 1985). The variation in exposure time measurements must be less than 10% for nominal exposure times shorter than 20 ms and less than 5% for nominal exposure times greater than 20 ms. Reproducibility of kV_p and exposure time measurements must be more than 95% for the range of checked values (Rossi *et al* 1985).

Target locating system x-ray generators: kV exposure output precision and linearity. In ordinary kV installations, radiation output is expressed in terms of mR per mAs and is used for the manual preparation of technique charts and in the calculation of patient exposure. AAPM report 74 (Shepard *et al* 2002) recommends that mR mAs^{-1} for all tube current settings on any given focal spot at any voltage setting must be within 20% throughout the entire range of tube current settings available for that focal spot. It also recommends that kV beam output in mR mAs^{-1} should be reproducible to within a coefficient of variation of 0.1. Exposure linearity between all mA or mAs settings must be within 10% (Rossi *et al* 1985), i.e.,

$$linearity = \frac{\left[\frac{mR}{mAs}\right]_{max} - \left[\frac{mR}{mAs}\right]_{min}}{\left[\frac{mR}{mAs}\right]_{max} + \left[\frac{mR}{mAs}\right]_{min}} \leqslant 0.10. \tag{2}$$

Target locating system x-ray generators are of constant load type with 2.5 mm Al inherent filtration, and in clinical practice, they operate with an appropriate field size that covers the detectors' surface.

Kilovoltage exposure output precision and linearity were measured with a high precision diagnostic electrometer connected to a solid-state detector with flat energy response and calibrated in kV diagnostic beams (DIADOS E T11035 electrometer, T60004 solid state detector, PTW, Freiburg, Germany). The solid-state detector was positioned at the isocenter facing the tested x-ray tube. At selected kV settings (80 kV to 120 kV) and constant exposure time of 100 ms, a set of exposures (mR) was performed for mAs values ranging from 5 mAs to 30 mAs by independently changing the mA setting. Each set of measurements at the specific kV setting and mAs value was repeated three times.

Target locating system cameras: image quality of flat-panel detectors. The flat-panel amorphous silicon detectors are situated at approximately 140 cm (depending on the ceiling height) from the isocenter and at a 45° angle to the kV-beam central axes (Fu and Kuduvalli 2008). They consist of a 1024×1024 pixel matrix of 0.4 mm nominal pixel size.

As a result of the horizontal installation, primary x-ray images suffer from a geometrical distortion of the projected object. This distortion is corrected by software based on the geometrical configuration of the target locating system cameras. The image quality of flat-panel detectors in terms of geometrical distortion and spatial resolution was evaluated using the ETR-1 multi purpose test tool (Scanditronix, Wellhöfer, Germany).

Each camera was tested individually with the ETR-1 tool positioned with its plane normal to the kV-beam central axis and centered at the imaging center. X-ray images from each camera were acquired using typical clinical parameters, i.e. 120 kV, 100 mA, 0.1 s, and further evaluated in tagged image file format (TIFF).

Geometrical distortion was qualitatively analyzed on the acquired images of the ETR-1 grid pattern with orthogonal and diagonal marks. The spatial resolution of each detector was quantitatively evaluated in terms of the modulation transfer function (MTF) using the built-in resolution test pattern of the ETR-1 tool. Normalized MTF values in the range of 0.6 lp mm^{-1} to 4 lp mm^{-1} were calculated (Curry *et al* 1990, Droege 1983) and the critical frequency, f50%, was used as a measure of the spatial resolution of each flat-panel detector corresponding to 50% relative normalized MTF value.

2.3. Linac performance and beam properties

2.3.1. Linac beam–laser beam axes coincidence. Linac beam and laser beam coincidence was evaluated by measuring the coincidence of the radiation field center and the laser beam spot on a plane normal to the central beam axis. The Gafchromic® EBT film (Lot#: 35322-004I, size $8'' \times 10''$) was irradiated at 12 different places using the whole set of system collimators. Initially, the film was positioned horizontally at the source-to-film distance (SFD) equal to SAD, thus, SFD = SAD = 800 mm, and in-between solid water slabs (RW3 solid water phantom, PTW, Freiburg, Germany) at 15 mm depth and 75 mm total thickness. Irradiations with programmed doses ranging from 300 MU to 400 MU were performed, so that similar exposures were produced on the film for each collimator size. Prior to each irradiation, the laser spot was marked on the film using a thin marker. This procedure was repeated for SAD = 650 mm and SAD = 1000 mm also in order to evaluate the linac–laser beam axes coincidence with other SADs. Following the irradiation, films were scanned using a calibrated flatbed optical scanner (Epson Expression 1680 Pro) in the presence of a non-irradiated background film and film images were acquired (300 dpi spatial resolution, 16 bit grayscale TIFF). A net pixel value matrix was obtained for each radiation field by subtracting the background signal in a pixel-by-pixel basis. The distance, dRL, between the Cartesian coordinates of the radiation field center and the laser beam spot on the net pixel value matrix of each field was

measured. The centroid method was used to find the coordinates of both the radiation field center and the laser beam center.

2.3.2. Beam quality. The beam quality of the 6-MV CyberKnife linac beam was specified in terms of the TPR^{20}_{10} beam quality index, according to the recommendations of the IAEA TRS-398 code of practice (Andreo *et al* 2000). The beam quality index TPR^{20}_{10} was measured with a waterproof 0.6 cm^3 Farmer ionization chamber (TW30013, PTW, Freiburg, Germany) placed at $d_1 = 10$ cm and $d_2 = 20$ cm in water. The source–detector distance (SDD) was equal to 1000 mm for the largest, 60 mm collimator.

2.3.3. Beam characteristics. Off-axis ratio (OAR) beam profiles were measured in a motorized water phantom (MP3, PTW, Freiburg, Germany) for the entire set of collimators (Nath *et al* 1994, Schell *et al* 1995, Duggan and Coffey 1998, Heydarian *et al* 1996). The PTW T60008 shielded diode detector (1 mm^2 cross section and 2.5 μm thickness of active layer), positioned in vertical direction, was used as a field detector. Beam profiles were taken at isocentric setup, i.e. SDD = SAD = 800 mm, and at depths 15 mm, 50 mm, 100 mm and 300 mm along two vertical diameters of each circular radiation field.

2.3.4. TMR measurements. TMR curves were measured in water (PTW MP3 motorized water phantom) for the whole set of system collimators for depths ranging from 0 mm up to 300 mm at isocentric setup, i.e. SDD = 800 mm. Point measurements were taken with the PTW T60008 shielded diode positioned in vertical direction. All curves were normalized to the 15 mm value resulting in TMR curves.

2.3.5. Output factors. The relative output factor is defined as the ratio of the radiation output for a given collimator to that of the 60 mm collimator. In the present work, the output factors were measured using the PTW T60008 shielded diode connected to a PTW UNIDOS electrometer. The diode was positioned vertically at a 15 mm depth in water and at an isocentric setup, i.e. SDD = SAD = 800 mm.

2.3.6. Beam output calibration. In the current study, a Farmer ionization chamber (T31013, 0.6 cm^3, PTW Freiburg, Germany) connected to a PTW UNIDOS electrometer was used to calibrate the 6-MV linac beam output for the 60 mm collimator. The Farmer chamber, calibrated in terms of absorbed dose in water, $N_{D,w}$, according to IAEA TRS 398 code of practice (Andreo *et al* 2000) was positioned horizontally at 50 mm depth in water with SSD = 750 mm and SDD = SAD = 800 mm. The absorbed dose at 50 mm depth was calculated according the IAEA TRS-398 code of practice. Using the appropriate TMR value, the measured dose at 50 mm was converted to the corresponding dose at 15 mm in water.

2.3.7. Output reproducibility, linearity and constancy versus linac orientation. Beam output reproducibility, linearity and constancy versus linac orientation are typical quality assurance procedures recommended by codes of practice (Nath *et al* 1994, AAPM TG40, IPEM etc). A special mounting facility (birdcage), provided by the vendor, was attached to the linac head. The birdcage was used to support horizontally a Farmer ionization chamber fitted with a 6-MV buildup cap and connected to a PTW UNIDOS electrometer at SAD = 800 mm. A set of ten measurements of 100 MU was performed using the 60 mm collimator. Beam output precision is defined as relative to the percent standard deviation of the measured

mean dose. Another set of ten measurements ranging from 5 MU to 1000 MU was performed and the linearity of beam output was calculated as the ratio of the measured dose for a specific number of delivered MU to the corresponding dose for 100 MU. Output constancy versus linac orientation was evaluated by performing a series of irradiations at different linac pointing orientations such as vertical upward, vertical downward, horizontal left, horizontal right, head up and head down. The output constancy was obtained as the ratio of the measured dose at any given orientation to that at the vertical–downward orientation. Beam profile constancy versus linac orientation was also checked at the four major clinical linac pointing orientations, i.e. vertical downward, horizontal left, horizontal right and head down. The Gafchromic EBT film was positioned normal to the central beam axis at source–film distance equal to SAD, SFD = SAD = 800 mm, and in-between solid water slabs at 50 mm depth and 150 mm total thickness.

2.3.8. Collimator transmission.   The system set of twelve collimators and a blank one are made of tungsten alloy (95% W, 1.5% Cu, 3.5% Ni by weight). A set of measurements with the Farmer chamber mounted on the birdcage was performed for the whole set of collimators. The collimator transmission was calculated as the ratio of the measured dose for each collimator to the dose measured with the blank.

2.3.9. End effect in treatment mode.   The end effect in treatment mode was evaluated. An isocentric plan (29 beams, 20 mm collimator, 2000 cGy prescribed dose) was created and delivered, using the fiducial tracking method, on solid water phantom slabs of 100 mm total thickness. A pinpoint ionization chamber (TW31014, 0.015 cm^3, PTW Freiburg Germany) connected to a UNIDOS electrometer inserted into an appropriately adapted solid water slab, at 50 mm depth and used to measure the delivered dose. The treatment was delivered twice, as non-interrupted and intentionally interrupted, and the dose measured in both modes was compared.

2.4. Accuracy of G4 CyberKnife SRS system

2.4.1. Phantom measurements for accuracy evaluation.   Dose placement measurements, i.e., accuracy, of the CyberKnife system were made for the fiducial, 6D skull and Xsight spine tracking methods using a head–neck anthropomorphic phantom (Mocel RS-108T, Radiological Support Services, Long Beach, CA, USA).

The head–neck phantom consists of a cranium and seven cervical vertebrae and contains two specially designed ball cubes/film holders, each designed to represent intracranial and spine lesions for quality assurance purposes (Yu *et al* 2004a, Ho *et al* 2007) (figures 1(a), (b)). Both ball cubes are constructed of acrylonitrile–butadiene styrene plastic containing an acrylic sphere in the cube's center with a higher CT number than the surrounding material.

The intracranial ball cube measures 63.5 mm on edge and contains a 31.75 mm diameter acrylic sphere in its center (figure 1(c)) (Accuray Physics Essentials 2006). The spine ball cube measures 31.75 mm on edge and contains a 19 mm acrylic sphere in its center (figure 1(d)).

The sphere center is within 0.13 mm of both cube centers as measured with optical techniques (Yu *et al* 2004a, Ho *et al* 2007, Accuray Physics Essentials 2006). Each ball cube serves as a film holder made of four identically shaped plastic rectangles. When the film holder is assembled, it holds two pieces of orthogonally positioned radiochromic dosimetry film in a known spatial relationship to the acrylic sphere (precut MD55, Gafchromic®, ISP Technologies, Wayne, NJ). To mark the position of the film precisely, the edges of the film are
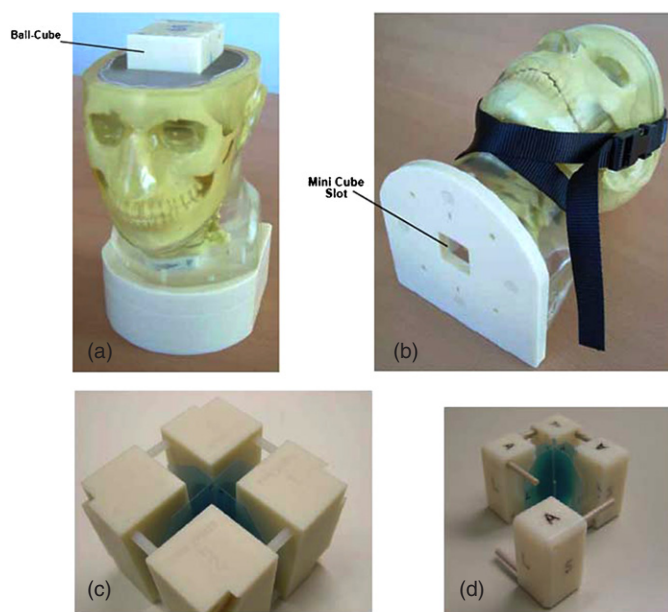
Figure 1. Head and neck phantom with intracranial and spine ball cubes used to evaluate targeting accuracy and precision of the G4 CyberKnife SRS system.

(This figure is in colour only in the electronic version)

aligned with the outer anterior, left and superior edges of the film holder. The film holder is oriented with the radiochromic film placed in axial and sagittal planes. The phantom with the film cube inside was imaged with a CT scanner (Siemens Somatom Definition CT scanner) with the following acquisition parameters: 120 kV tube voltage, 512×512 pixels matrix size, 300 slices, 1 mm slice thickness, no interslice gap, field of view 250×250 mm^2. Although accuracy of the CyberKnife system has been proven to be independent of the slice thickness in the range of 1–1.5 mm (Yu *et al* 2004a, Ho *et al* 2007), the 1 mm slice thickness is used in all phantom and patient scanning protocols in our department.

Phantom CT images are DICOM-imported into the treatment planning system (TPS) (Cyris Multiplan v2.01, Accuray Inc.). The acrylic sphere target is then delineated using the TPS and a respective treatment plan is designed. The phantom with the film cube inside is then treated normally, i.e. exposing the film to the pre-designed plan. Delivery of the pre-designed plan was performed using each one of the tracking methods. At least 24 h after the irradiation, the self-developing radiochromic films were scanned in a flatbed transparency optical scanner (EPSON Expression 1680 Pro) together with a non-irradiated film of the same batch. Film images were acquired (300 dpi spatial resolution, 16 bit grayscale) and stored in TIFF. Net optical density in each film was calculated by subtracting the background on a pixel-by-pixel basis. The centroid method was used to find the center of the relative optical density distribution and the corresponding delivered dose distribution using a threshold value of 70%, which matches the isodose encompassing the delineated sphere target during the treatment planning process.

Dose placement accuracy is defined as the offset between the centroid of the delivered dose distribution and the center of the respective sphere target located in the phantom with the

selected dose contour matching the sphere diameter. Details on the film analysis procedure and targeting error evaluation are given in the literature (Chang *et al* 2003, Yu *et al* 2004a, Ho *et al* 2007).

2.4.2. Performance of the image guidance system and beam delivery precision. Treatment delivery precision of the CyberKnife image-guided robotic SRS system is associated with the collaborating performance of the robot and the imaging system. It represents the ability of the system to track any offset in patient's position and then to realign the linac beam to that offset position. It is defined as the beam delivery precision using the image guidance system. Measurements of dose placement, as defined above, were made by delivering repeatedly the same treatment plan on the same phantom. In each delivery/measurement, the phantom was optimally aligned for treatment and then it was deliberately offset by 8 mm along each coordinate axis. The head–neck phantom, described above, was used with the intracranial ball cube loaded with the radiochromic dosimetry film (Gafchromic®, MD55).

2.4.3. Total clinical accuracy. Evaluation of total clinical accuracy of the CyberKnife SRS system refers to an accuracy measurement of delivering a radiation dose to a target defined on a set of CT images using all components of the CyberKnife therapeutic procedure including the treatment planning system, software, the robot, the tracking system and the linear accelerator (Chang *et al* 2003).

Total clinical accuracy of our G4 CyberKnife system was evaluated for 6D skull, fiducial and Xsight spine tracking methods. Measurements were performed using the head–neck phantom and delivering pre-designed treatment plans for each tracking method, as described above. This measurement mode gives the total error expected in a patient treatment, because each test includes a unique set including a CT scan, a treatment plan and treatment delivery; thus both localization and delivery errors are included.

Five treatment plans were created for each tracking method. A total dose of 2400 cGy at the 70% isodose line encompassing the diameter of the acrylic sphere in the respective ball cube was administered in each individual plan. The irradiated films were scanned and analyzed as described above.

Total clinical accuracy of the CyberKnife SRS system for each tracking method was considered to be equivalent to the mean dose placement accuracy measured in each individual test, i.e., the offset between the centroid of the delivered dose distribution and the center of the targeting sphere located in the phantom with the selected dose contour covering the diameter of the sphere.

3. Results

3.1. Quality control of the CyberKnife subsystems

3.1.1. Manipulator mechanical accuracy. Measurements were taken for all the available treatment paths of our CyberKnife system and the respective mean $\overline{dr}$ and maximum dr_{max} radial displacement errors are presented in table 1.

As shown in table 1, the mean radial displacement error of the manipulator for all treatment paths was less than 0.1 mm, whereas the individual maximum error never exceeded 0.29 mm for any of the treatment paths.
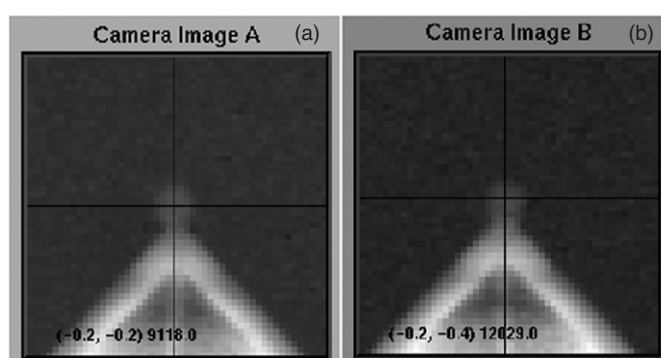
Figure 2. (a), (b) X-ray images of the isocrystal defining the imaging center.

Table 1. Mean ($\overline{dr}$) and maximum (dr_{max}) displacement errors for the available treatment paths of our CyberKnife system.

Treatment path	No. of nodes	$\overline{dr}$ (mm)	dr_{max} (mm)
Head path 1	124	0.10 ± 0.04	0.24
Head path 2	72	0.08 ± 0.04	0.24
Head path 3	127	0.10 ± 0.04	0.25
Head path 4	138	0.11 ± 0.05	0.27
Body path 1	108	0.08 ± 0.04	0.24
Body path 2	68	0.08 ± 0.05	0.20
Body path 3	111	0.10 ± 0.05	0.29

3.1.2. Target locating system performance evaluation.

Mechanical accuracy of target locating system cameras' alignment. Acquired images for both cameras A and B with the isopost mounted on the treatment room floor are presented in figure 2.

Coordinates of the projected isopost, depicted by the cross hairs in the images, were measured to be (-0.2 mm, -0.2 mm) and (-0.2 mm, -0.4 mm) for cameras A and B, respectively. The measured coordinate values were therefore less than ± 1 mm in both directions, and so the target locating system mechanical alignment was found to be acceptable for our system.

Target locating system x-ray generators: accuracy and precision of kV and exposure time settings. A set of measurements was taken in the range of 60–120 kV and 20–500 ms. Accuracy and precision for each type of measurement were calculated. The measured data and results for both tubes' kV measurements are presented in table 2.

The measured data and results for exposure time measurements are presented in table 3. The results in table 2 showed kV accuracy ranging from 10% for the 60 kV nominal value to 0.2% for the 120 kV nominal value. The corresponding results of exposure time measurements showed a deviation from time-setting accuracy ranging from 4% for the 20 ms nominal value to 0.2% for the 400 ms nominal value. Kilovoltage and exposure time precision was found to be better than 1% relative to the corresponding kV and exposure time nominal

Table 2. Accuracy and precision results of kV settings of the target locating system x-ray generators.

mA	60 kV$_{nom}$ accuracy (%)		80 kV$_{nom}$ accuracy (%)		100 kV$_{nom}$ accuracy (%)		120 kV$_{nom}$ accuracy (%)	
	Unit A	Unit B	Unit A	Unit B	Unit A	Unit B	Unit A	Unit B
25	10.0	6.2	5.4	8.1	4.7	4.3	3.5	1.9
50	5.5	3.7	8.6	6.9	3.7	2.3	1.7	0.7
100	4.8	2.2	6.5	5.6	2.5	1.8	1.3	0.3
150	2.8	1.8	6.1	5.0	2.3	2.1	−0.5	−0.3
200	3.0	1.7	4.9	4.7	2.0	1.4	−0.4	−0.2
Precision (%)	0.25	0.41	0.14	0.30	0.20	0.30	0.13	0.13

Table 3. Accuracy and precision results of the exposure time settings of the target locating system x-ray generators.

(ms)	Unit A		Unit B	
	Accuracy (%)	Precision (%)	Accuracy (%)	Precision (%)
20	3.50	0.84	4.00	0.83
35	2.29	0.48	2.29	0.48
50	1.33	0.11	1.93	0.11
100	0.60	0.17	0.70	0.17
150	0.40	0.12	0.60	0.11
200	0.35	0.09	0.40	0.09
300	0.20	0.06	0.32	0.08
400	0.14	0.01	0.20	0.04

Table 4. kV exposure output linearity and precision values for the target locating system x-ray generators.

	Unit A			Unit B		
	80 kV mR mAs^{-1}	100 kV mR mAs^{-1}	120 kV mR mAs^{-1}	80 kV mR mAs^{-1}	100 kV mR mAs^{-1}	120 kV mR mAs^{-1}
Mean output (mR mAs^{-1})	1.08	1.76	2.50	1.10	1.77	2.48
Precision (mR mAs^{-1}) (%)	4.33	4.30	4.50	3.29	3.68	4.06
Linearity (%)	6.09	5.90	5.82	4.39	4.94	5.20

values. Accuracy and precision of kV and exposure time settings of the target locating system x-ray generators were within the acceptance limits followed in diagnostic radiology (Shepard *et al* 2002).

Target locating system x-ray generators: kV exposure output linearity and precision. Measured data for both target locating system x-ray generators are presented in table 4.

The kV output data were averaged for both generators and the mean kV output was found to be 1.9 mR mAs^{-1} for 80 kV, 1.8 mR mAs^{-1} for 100 kV and 2.5 mR mAs^{-1} for 120 kV (table 4). Linearity of kV exposure output, for x-ray tubes A and B, was found to be 6.1% and 4.4% at 80 kV, 5.9% and 4.9% at 100 kV, and 5.8% and 5.2% at 120 kV, respectively.
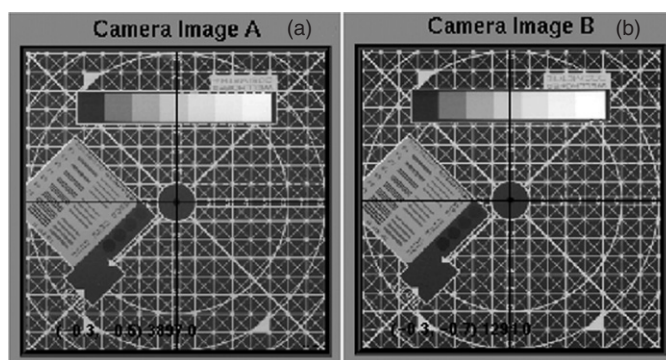
Figure 3. (a), (b) ETR images on cameras A and B. No geometrical distortion is observed.

Taking into account that the above data referred to in-air measurements and assuming a backscatter factor of 1.3 for 120 kV tube voltage (IPSM Report 53 1988), the patient's surface entrance dose due to kV imaging during a CyberKnife treatment session was found equal to 32.5 μGy mAs^{-1} per image acquisition. Considering a typical 10 mAs used per image acquisition and two images per acquisition, the cumulative patient surface entrance dose was estimated to be equal to 0.7 mGy per acquisition during a CyberKnife treatment session:

$$32.5 \frac{\mu \text{Gy}}{\text{mAs}} \times 10 \frac{\text{mAs}}{\text{image}} \times 2 \frac{\text{images}}{\text{acquisition}} = 0.7 \frac{\text{mGy}}{\text{acquisition}}.$$

Target locating system cameras: image quality of flat-panel detectors. Acquired images of the ETR tool are presented in figures 3(a) and (b) for detectors A and B, respectively. Qualitative analysis of the ETR-1 grid pattern with orthogonal and diagonal marks revealed no geometrical distortion on the images with either detector.

Spatial resolution of each detector was quantitatively evaluated in terms of MTF using the built-in resolution pattern of the ETR-1 tool (figure 3). Normalized MTF for frequency values in the range of 0.6 lp mm^{-1} to 4 lp mm^{-1} were calculated for both detectors (figure 4).

Both showed similar behavior in the studied frequency range with critical frequency, $f_{50\%}$, where the values of 1.5 lp mm^{-1} and 1.4 lp mm^{-1} were calculated for detectors A and B, respectively.

3.1.3. Linac performance and beam properties.

Linac beam–laser beam axes coincidence. Linac and laser beam axes coincidence in terms of dRL distance is presented in table 5 for all the system collimators and the three SADs.

Uncertainties of the dRL distances were calculated using the propagation analysis of the standard deviation of the mean coordinates for each radiation field. The results presented in table 5 showed that the coincidence of the linac and the laser beam axes was better than 0.4 mm in all tested cases.

Beam quality. Beam quality of the 6-MV CyberKnife linac beam was specified in terms of the TPR$^{20}_{10}$ beam quality index, according to IAEA TRS 398 code of practice. At SDD = 100 cm, the 60 mm circular field is projected equal to 75 mm circular field. The
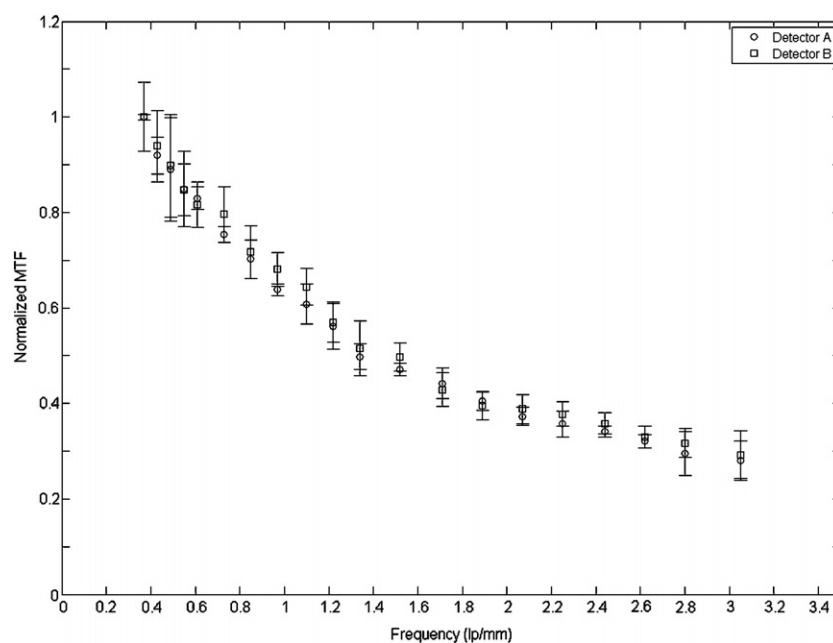
Figure 4. Normalized modulation transfer function values for the flat-panel detectors of the target locating system as a function of frequency in lp mm^{-1}.

Table 5. Treatment–laser beam axes coincidence, dRL, results for the available collimator sizes of the system and 65 cm, 80 cm and 100 cm SAD values.

	Axes coincidence, dRL (mm)		
Collimator	SAD = 65 cm	SAD = 80 cm	SAD = 100 cm
5	0.14 ± 0.03	0.16 ± 0.02	0.17 ± 0.03
7.5	0.21 ± 0.04	0.27 ± 0.02	0.30 ± 0.04
10	0.35 ± 0.03	0.33 ± 0.03	0.35 ± 0.03
12.5	0.21 ± 0.02	0.20 ± 0.03	0.25 ± 0.04
15	0.35 ± 0.04	0.38 ± 0.04	0.39 ± 0.05
20	0.26 ± 0.02	0.27 ± 0.03	0.28 ± 0.04
25	0.15 ± 0.03	0.13 ± 0.02	0.14 ± 0.03
30	0.20 ± 0.04	0.22 ± 0.04	0.21 ± 0.05
35	0.25 ± 0.03	0.29 ± 0.03	0.30 ± 0.03
40	0.29 ± 0.02	0.30 ± 0.01	0.31 ± 0.02
50	0.19 ± 0.02	0.19 ± 0.02	0.20 ± 0.03
60	0.13 ± 0.02	0.12 ± 0.04	0.15 ± 0.05

equivalent square field is then equal to 67 mm $\times$ 67 mm. A TPR$^{20}_{10}$ value of 0.657 was measured at SDD = 1000 mm for the 60 mm circular collimator. This value was in excellent agreement with the corresponding value of 0.655 obtained for the equivalent square field of the 60 mm circular field and linear interpolation of square field data reported in BJR Supplement No 25 (Aird *et al* 1996).
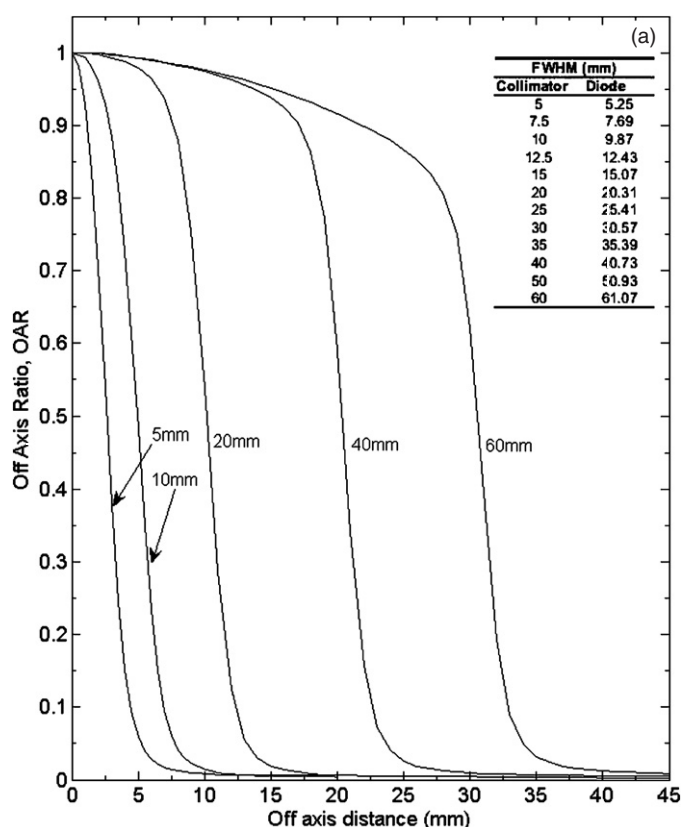
FWHM (mm)	
Collimator	Diode
5	5.25
7.5	7.69
10	9.87
12.5	12.43
15	15.07
20	20.31
25	25.41
30	30.57
35	35.39
40	40.73
50	50.93
60	61.07

Figure 5. OAR beam profiles versus off-axis distance and (a) the corresponding FWHM values of the measured profiles for the available system collimators.

Beam characteristics. Beam profiles were taken at an isocentric setup, i.e. SAD = 800 mm, and at depths of 15 mm, 50 mm, 100 mm and 300 mm along two vertical diameters of each circular field. Half-beam profiles were produced by averaging four symmetrical measured profiles around the field center and normalizing to the corresponding central value. Half-beam profiles at 15 mm depth of the 5 mm, 10 mm, 20 mm, 30 mm, 40 mm and 60 mm collimators are presented in figure 5.

The measured profiles presented in figure 5 show similar steep dose gradients and a flattened region that is absent with the small collimators (5–7.5 mm). FWHM for all measured OAR profiles was also calculated (figure 5(a)). FWHM values were also in good agreement (within 2%) with the corresponding nominal values of each collimator, except for the 5 mm and 7.5 mm collimators, where a deviation up to 5% was observed.

TMR measurements. TMR curves were measured in water for all the system collimators for depths ranging from 0 mm to 300 mm. The TMR curves for the 5 mm, 10 mm, 20 mm, 30 mm, 40 mm and 60 mm collimators are presented in figure 6.

The well-known behavior of high energy beam attenuation versus collimator size could be observed with increasing TMR values with increasing collimator size. A slight shift of the depth of the maximum dose toward deeper points up to 17 mm for the 60 mm collimator was also observed.
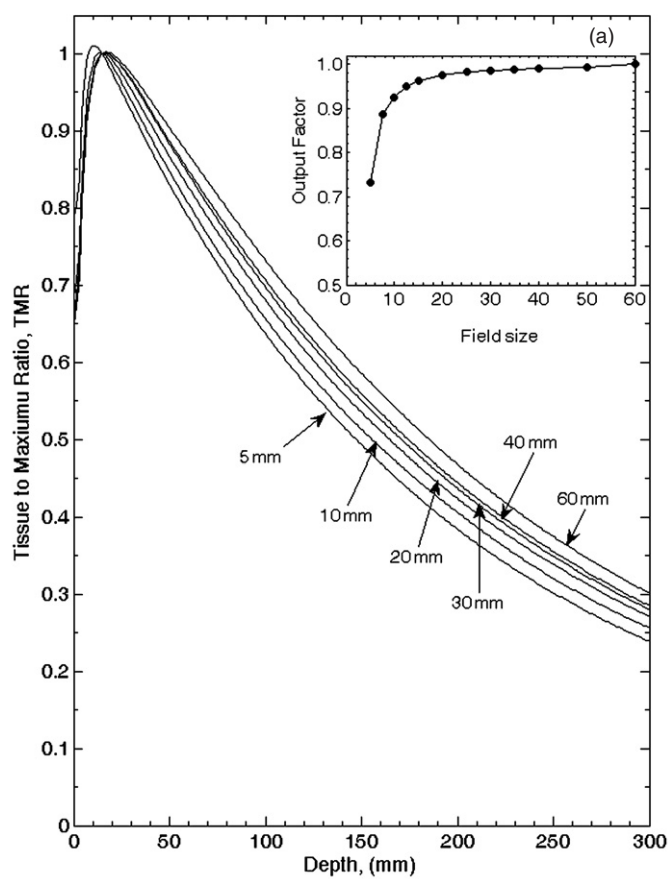
Figure 6. TMR versus depth for the available field sizes of the system. In the inset (a) the output factors versus field size are also presented.

Output factors. Relative output factors for all the system collimators were measured with the PTW T60008 shielded diode detector. These were then normalized relative to the 60 mm collimator and presented in figure 6(a).

Beam output calibration. The CyberKnife 6-MV linac beam was calibrated to give 1 cGy per 1 MU at 15 mm depth in water with a Farmer ionization chamber at isocentric setup (SDD = SAD = 800 mm) for the 60 mm collimator. A calibration uncertainty of 1.2% was obtained as the square root of the sum in quadrature of the standard deviation of the measured mean charge (0.19%), chamber's calibration factor uncertainty (0.6%), condition correction factors uncertainty (0.3%) and the beam quality correction factor uncertainty (1%) (Andreo *et al* 2000).

Output precision, linearity and constancy versus linac orientation. Precision uncertainty for the 100 MU set of measurements was found to be less than 0.5%, whereas linearity variation for the whole range of measured MUs was also determined to be less than 0.3%. Beam output constancy versus linac orientation was found better than 0.6% compared with the vertical
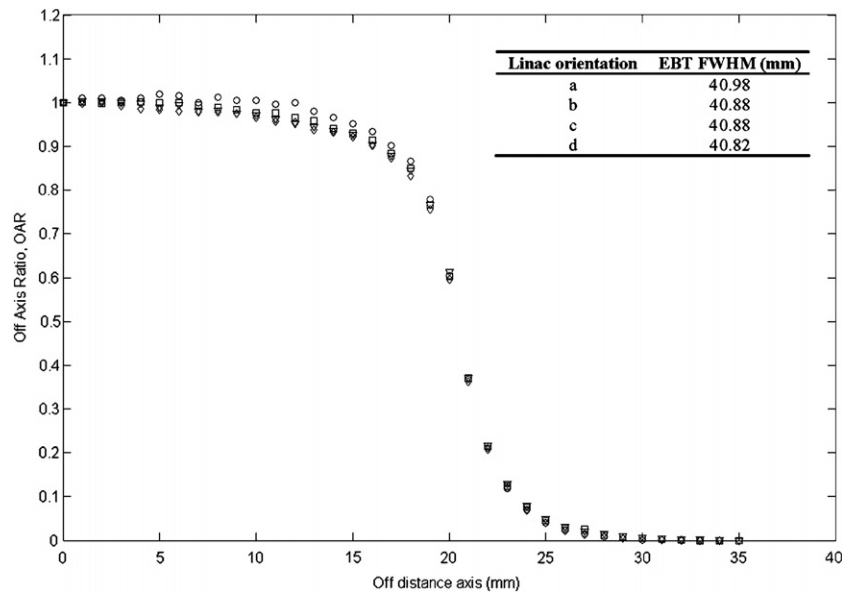
Linac orientation	EBT FWHM (mm)
a	40.98
b	40.88
c	40.88
d	40.82

Figure 7. Beam profiles measured at four major clinical linac orientations: (a) vertical downwards, (b) horizontal left, (c) horizontal right and (d) head down.

downward linac orientation. Half beam profiles at the four major clinical linac orientations are presented in figure 7. FWHM of beam profiles remains constant for all measured orientations.

Collimator transmission. Collimator transmission for each of the system collimators was measured to be lower than 0.14%.

End effect in treatment mode. An isocentric plan (29 beams, 20 mm collimator, 2000 cGy prescribed dose) was delivered in treatment modes and in two separate ways: non-interrupted and interrupted into two parts (first part: delivery of 15 beams; second part: delivery of remaining 14 beams). The absorbed dose measured in both ways (non-interrupted and interrupted) agrees to within 0.5%.

3.2. Accuracy of G4 CyberKnife SRS system

3.2.1. Beam delivery precision. Beam delivery precision was evaluated with dose placement measurements. A treatment plan with fiducial tracking method was designed. Along with the correctly aligned position at the nominal isocenter, six other administrations of the same treatment plan were performed with the head–neck phantom positioned with an 8 mm offset along each coordinate axis for each measurement.

Dose placement accuracy was measured in terms of anterior/posterior (A/P), left/right (L/R) and superior/inferior (S/I) error components. The root mean square (RMS) of the three error components was considered to represent the total error in the dose placement accuracy. Likewise, the average total error of all delivery trials was considered to be the beam delivery precision uncertainty of our CyberKnife system with fiducial tracking. Error components and total error of dose placement accuracy of each trial are presented in table 6.

Table 6. Total and individual error component dose placement accuracy results with and without phantom offset using fiducial tracking algorithm.

Trial	Phantom offset	A/P (mm)	L/R (mm)	S/I (mm)	Accuracy (mm)
1	0	0.08	−0.07	−0.16	0.19
2	ANT = 8 mm	−0.15	0.27	−0.28	0.41
3	POST = 8 mm	0.11	0.15	0.05	0.20
4	LEFT = 8 mm	0.16	0.09	0.04	0.18
5	RIGHT = 8 mm	0.05	−0.01	−0.06	0.08
6	SUP = 8 mm	0.28	−0.16	−0.02	0.32
7	INF = 8 mm	−0.06	0.22	−0.11	0.25
	Average	0.07	0.07	−0.08	0.23
	SD	0.14	0.16	0.12	0.11
	No offset accuracy	0.08	−0.07	−0.16	0.19
	Offset accuracy	0.06	0.09	−0.06	0.24
	SD	0.15	0.16	0.12	0.12

The average error in beam delivery precision with fiducial tracking was 0.23 ± 0.11 mm; the single measurement no-offset error was 0.19 mm; and the average offset error was 0.24 mm. The measured errors revealed submillimeter beam delivery precision when tracking fiducials.

3.2.2. Total clinical accuracy. Table 7 summarizes the measurement data and the mean total accuracy results for each tracking method.

Presented data reveal submillimeter accuracy for all tracking methods. The fiducial tracking method was found to present the finest accuracy of 0.29 ± 0.10 mm whereas the 6D skull and Xsight tracking methods present accuracy of 0.49 ± 0.17 mm and 0.53 ± 0.16 mm, respectively.

4. Discussion

The aim of the current work was to present the performance evaluation procedures implemented at our department for the commissioning of a G4 CyberKnife system. This system consists of a robotic manipulator, a target locating system and a lightweight 6-MV linac. Individual quality assurance procedures were performed for each of the CyberKnife subsystems.

First, the system was checked for the mechanical accuracy of the robotic manipulator. It was found capable of pointing the linac beam to predefined nodes with a mean mechanical accuracy of 0.1 ± 0.04 mm with maximum individual position uncertainty being less than 0.25 mm.

Performance of the target locating system was evaluated in terms of mechanical accuracy of both cameras' alignment and quality assurance tests of the x-ray generators and the flat-panel detectors. Target locating system cameras' alignment was measured to be accurate within ± 1 mm in both directions of camera images. Good coincidence of the target locating system and manipulator frame origins was revealed, which further suggests the accurate transformation of the imaging object points from the target locating system coordinate frame into the manipulator workspace coordinates (Murphy and Cox 1996). The kV parameters were checked for both x-ray generators. In all measured cases, our results are within the

Table 7. Clinical accuracy results for the 6D skull tracking, fiducial tracking and Xsight spine tracking algorithms of our CyberKnife system.

Trial	A/P (mm)	L/R (mm)	S/I (mm)	Accuracy (mm)
6D skull tracking—clinical accuracy				
1	0.25	−0.52	−0.16	0.60
2	0.23	0.40	−0.04	0.46
3	0.24	−0.25	−0.19	0.40
4	0.29	0.09	−0.36	0.47
5	0.20	0.11	−0.16	0.28
Average	0.24	−0.04	−0.18	0.44
SD	0.03	0.35	0.11	0.12
Fiducial tracking—clinical accuracy				
1	0.17	−0.22	−0.07	0.29
2	0.06	−0.06	−0.38	0.39
3	−0.03	0.11	0.03	0.12
4	0.31	−0.14	−0.07	0.34
5	−0.13	−0.06	−0.29	0.32
Average	0.08	−0.07	−0.16	0.29
SD	0.17	0.12	0.17	0.10
XSS spine tracking—clinical accuracy				
1	−0.42	0.27	−0.22	0.54
2	−0.09	−0.57	−0.12	0.59
3	0.04	−0.24	−0.04	0.24
4	0.01	−0.61	0.06	0.61
5	0.13	0.25	−0.59	0.65
Average	−0.06	−0.18	−0.18	0.53
SD	0.21	0.43	0.25	0.16

acceptable limits and specifications recommended by quality assurance protocols used in diagnostic radiology (Shepard *et al* 2002). Accuracy and precision of kV and exposure time settings were measured. For both measured parameters, accuracy deviation was found to be less than 10% and precision deviation to be less than 1%. The maximum deviations were measured for small nominal values, e.g., 60 kV (max 10% deviation) and 40 ms (max 4% deviation). For parameters clinically used the most in CyberKnife practice, e.g., 100 kV–120 kV and 50 ms–200 ms, deviation from accuracy was measured less than 2%. The kV output linearity and precision were spot checked at selected kV settings and in a wide range of mAs values. For the most clinically used parameters in CyberKnife practice, deviation from kV output linearity was measured less than 6% and from precision less than 5%. Generator A's precision was found to be less than that of generator B, but within acceptable limits.

Image quality of target locating system flat-panel detectors was evaluated qualitatively and quantitatively using a radiographic test tool. The horizontal positioning of the flat detectors results in a geometrical distortion of the primary x-ray images, which are then corrected by the image registration algorithm (Fu and Kuduvalli 2008). Test tool images were acquired under clinical conditions, i.e., with the test tool positioned at the imaging center and its plane normal to the kV beam central axis. Qualitative analysis of the tool grid panel revealed no geometrical distortion on either detector image. Therefore, it can be stated that the horizontal

positioning does not affect the quality of the reconstructed images of any projected objects. Nevertheless, further investigation is required in order to quantitatively evaluate geometrical distortion of the target locating system images.

Spatial resolution of each detector was evaluated in terms of normalized MTF for frequency values in the range of 0.6 lp mm^{-1} up to 4 lp mm^{-1}. The critical frequency f_{50} was calculated to be 1.5 lp mm^{-1} and 1.4 lp mm^{-1} for detectors A and B, respectively. The measured f_{50} values were higher than the 0.4 mm physical spatial resolution of the flat-panel detectors. This could be attributed to the longer distance ($\sim$140 cm) between the imaging center and the detectors, which might have resulted in a decrease in the sharpness of the imaged object due to an increase in scattered radiation reaching the detectors. However, we believe that these are realistic values since they emulate the clinical conditions under which CyberKnife treatments are performed.

Procedures for the commissioning of the imaging target locating system, presented in this work, were performed by the authors and they are not included in the commissioning and acceptance-testing procedures recommended by the vendor (Accuray Physics Essentials 2006). We believe that the consistent performance of the target locating system is of great importance to the overall performance of the system under investigation. Further investigation should be done in order to examine the influence of any instability of the imaging sub-system on the overall performance of the CyberKnife system itself. Taking into account that the target locating system cameras, x-ray generators and the flat-panel detectors are not used for diagnostic purposes but nevertheless are part of the image-guidance system of a SRS system, we believe that more stringent acceptable limits should be used. Considering that the overall accuracy of any image-guided system is based, to a great extent, on the performance and consistency of the imaging system, we recommend reducing the acceptable limits of accuracy to 5%, precision to 2% for the x-ray parameters; kV output linearity and precision to 5% and 2%, respectively. Quality assurance of x-ray generators and image quality of the flat-panel detectors should be performed during acceptance of the system and periodically checked thereafter.

Evaluation of the linac performance should include all the traditional quality assurance procedures modified for the CyberKnife linear accelerator. In CyberKnife, although there is no light field representing radiation field, the linac beam axis and pointing direction are represented by a laser beam of diameter 1 mm. Linac and laser beam axes coincidence was evaluated by means of Gafchromic EBT film, irradiated at 12 different locations using the whole system collimator set at three different SADs. In addition to the visual inspection of the irradiated film, we suggest a quantitative analysis for this test. The coincidence of the axes was calculated as the distance, dRL, of the Cartesian coordinates of the centroids of the radiation field from the laser beam spot. Our results revealed a submillimeter coincidence between axes for all system collimators and at all checked SADs. Traditionally, small field dosimetry measurements were performed for the commissioning of the system. Dosimetric beam characteristics such as beam quality, beam profiles, TMR measurements and, finally, output factors for the whole set of system collimators were measured. Lack of electronic equilibrium and the finite dimensions of the detectors compared with the radiation field had to be taken into account. Small field dosimetry is considered a challenging field in itself and there are numerous publications on the small field dosimetry and output factor measurements with various dosimetric means for various SRS systems, including the Gamma Knife and XKnife (Heydarian *et al* 1996, Pappas *et al* 2005, 2006, Karaiskos *et al* 2005). Moreover, Francescon *et al* (2005) compared experimental results and Monte Carlo simulation of the CyberKnife linac beam and recently Pantelis *et al* (2008) used 3D polymer gels to dosimetrically characterize the CyberKnife linac beam. However, it was beyond the scope of the current work to investigate

deeply and in detail the dosimetric characteristics of the CyberKnife linac beam. Our aim was merely to present a complete series of quality assurance procedures and dosimetric measurements that should be performed for the commissioning of the system with reliable means. From this point of view, only experimental results using the diode detector were presented and no comparison with other dosimetric equipment was investigated for this work.

Dose placement measurements were made using a head–neck phantom with two pre-cut MD55 radiochromic films in orthogonal configuration loaded into respective ball cubes. Beam delivery precision was first investigated and represented the ability of the system to track any offset in patient position and to compensate for the displacement. The average error in beam delivery precision with fiducial tracking was measured 0.23 ± 0.11 mm, whereas the error in the single measurement with no-offset was 0.19 mm and the average offset error was 0.24 mm (table 6). Beam delivery precision of previous CyberKnife generations has been investigated by other authors. Chang *et al* (2003) investigated the G2 system and they measured an average 8 mm offset accuracy equal to 0.64 mm compared to the no-offset accuracy of 0.52 mm using the skull tracking method. Yu *et al* (2004a) investigated the G3 system and they measured an average 8 mm offset accuracy of 0.28 mm ± 0.11 mm using the fiducial tracking method. Our results on beam delivery precision are improved compared to the G2 system and are almost identical to the G3 system results where the same tracking method was used. The above results demonstrate submillimeter targeting accuracy, which indicates that the image guidance efficiency of the CyberKnife system was not significantly affected by the patient position inside the maximum allowed targeting space of ± 10 mm.

Total clinical accuracy is considered the total error expected in the patient treatment and includes all error components associated with each individual step of the treatment procedure, i.e., imaging, treatment planning and treatment delivery. To evaluate the total accuracy of our G4 system, the whole treatment process was repeated five times for each tracking method. Averaged data, presented in table 7, showed a mean accuracy of 0.44 ± 0.12 mm for skull tracking, 0.29 ± 0.10 mm for fiducial tracking and 0.53 ± 0.16 mm for Xsight spine tracking. The above results demonstrate that the evaluated G4 CyberKnife system is able to implement stereotactic treatments with sub-millimeter clinical accuracy. The G2 system total clinical accuracy has been investigated by Chang *et al* (2003) for skull tracking at various CT slice thicknesses. They report an error level of 0.68 ± 0.29 mm for 0.625 mm slice thickness and 1.1 ± 0.3 mm for 1.25 mm slice thickness. The G3 system total clinical accuracy has been investigated by Yu *et al* (2004a) for fiducial tracking. It was found to be independent of CT slice thickness and equal to 0.7 ± 0.3 mm. The G3 system's total clinical accuracy for Xsight spine tracking has been investigated by Ho *et al* (2007) and Muacevic *et al* (2006). They report an accuracy within 0.61 ± 0.2 mm and 0.52 ± 0.22 mm, respectively for 1 mm slice thickness. The total clinical accuracy of the investigated G4 system was found to be improved for the skull and fiducial tracking methods and was comparable for the Xsight spine tracking method compared with the earlier generation of the instrument.

5. Conclusions

We have carried out certain performance evaluation procedures for a G4 CyberKnife robotic stereotactic radiosurgery system. The system was checked for the mechanical accuracy of its robotic manipulator, its mechanical accuracy, image quality, kV parameters of the target locating system as well as for the traditional linac 6-MV beam characteristics and beam output parameters. The total accuracy of the system in positioning the dose distribution in a predefined point was evaluated for the skull, fiducial and Xsight spine tracking methods. The results revealed a manipulator mechanical mean accuracy of ~ 0.1 mm, with individual maximum

position uncertainties less than 0.25 mm. The target locating system mechanical accuracy was found within the acceptance limits. For the most clinically used parameters in the CyberKnife practice, e.g. 100–120 kV and 50–200 ms, kV and exposure time accuracy error were measured as less than 2%, while the precision error of the kV was determined as less than 1%. The acquired images of the ETR grid pattern revealed no geometrical distortion while the critical frequency f_{50} values for cameras A and B were calculated as 1.5 lp mm^{-1} and 1.4 lp mm^{-1}, respectively. Dose placement measurements were performed in a head and neck phantom. The results revealed sub-millimeter beam delivery precision whereas the total clinical accuracy of the system was measured equal to 0.44 ± 0.12 mm, 0.29 ± 0.10 mm and 0.53 ± 0.16 mm for the skull, fiducial and Xsight spine tracking methods, respectively. The results of this work certify the CyberKnife SRS system capable of delivering high dose distributions with sub-millimeter accuracy and precision to intracranial and extracranial lesions.

References

Accuray Physics Essentials Guide 2006 *Cyberknife System Manual* (Sunnyvale, CA: Accuray(tm) Inc.)

Adler J R, Murphy M J, Chang S D and Hancock S L 1999 Image-guided robotic radiosurgery *Neurosurgery* **44** 1299–307

Aird E G A *et al* 1996 Central axis depth dose data for use in radiotherapy *Br. J. Radiol.* Suppl. 25 (London: British Institute of Radiology)

Andreo P, Burns D T, Hohlfeld K, Huq M S, Kanai T, Laitano F, Smyth V and Vynckier S 2000 Absorbed dose determination in external beam radiotherapy: an international code of practice for dosimetry based on standards of absorbed dose to water *IAEA Technical Report Series 398* (Vienna: IAEA)

Bucholz R D, Gagnon, Gerszten P C, Kresl J J, Levendag P C, Schulz R A and Mould R F 2005 *Robotic Radiosurgery* vol 1 (Sunnyvale, CA: The CyberKnife Society Press)

Casamassima F, Cavedon C, Francescon P, Stancanello J, Avanzo M, Cora S and Scalchi P 2006 Use of motion tracking in stereotactic body radiotherapy: evaluation of uncertainty in off-target dose distribution and optimization strategies *Acta Oncol.* **45** 943–7

Chang S D, Main W, Martin D P, Gibbs I C and Heilbrun M P 2003 An analysis of the accuracy of the CyberKnife: a robotic frameless stereotactic radiosurgical system *Neurosurgery* **52** 140–6

Curry T S, Dowdey J E and Murry R C Jr 1990 *Christensen's Physics of Diagnostic Radiology* 4th edn (Philadelphia: Lea and Febiger)

Droege R T 1983 A practical method to routinely monitor resolution in digital imagers *Med. Phys.* **10** 37–43

Duggan D M and Coffey C W 1998 Small photon field dosimetry for stereotactic radiosurgery *Med. Dosim.* **23** 153–9

Francescon P, Cora S, Cavedon C, Scalchi P, Recannello and Colombo F 1998 Use of new type radiochromic film, a new parallel-plate micro-chamber, MSFETS and TLD 800 microcubes in the dosimetry of small beams *Med. Phys.* **25** 503–11

Francescon P, Cora S, Cavedon C, Scalhi P and Stancanello J 2005 *Cyberknife Dosimetric Beam Characteristics: Comparison Between Experimental Results and Monte Carlo Simulation Robotic Radiosurgery* Vol 1 (CyberKnife Society Press) pp 271–80

Fu D, Kuduvalli G, Mitrovic V, Main W and Thomson L 2005 Automated skull tracking for the CyberKnife image-guided radiosurgery system *SPIE Medical Imaging: Image Processing (2005, San Diego, CA)* pp 366–77

Fu D and Kuduvalli G 2008 A fast, accurate and automatic 2D–3D image registration for image-guided cranial radiosurgery *Med. Phys.* **35** 2180–94

Hansen E K, Larson D A, Aubin M, Chen J, Descovich M, Gillis A M, Morin O, Xia P and Pouliot J 2006 Image-guided radiotherapy using megavoltage cone-beam computed tomography for treatment of paraspinous tumors in the presence of orthopedic hardware *Int. J. Radiat. Oncol. Biol. Phys.* **66** 323–6

Heydarian M, Hoban P W and Beddoe A H 1996 A comparison of dosimetry techniques in stereotactic radiosurgery *Phys. Med. Biol.* **41** 93–110

Ho A K, Fu D, Cotrutz C, Hancock S, Chang S, Gibbs I R, Maurer C and Adler J R 2007 A study of the accuracy of spinal radiosurgery using skeletal structure tracking *Neurosurgery (Operative Neurosurgery)* **60** 147–56

IPSM 1988 Patient dosimetry techniques in diagnostic radiology *Report No. 53* (New York: IPSM)

Karaiskos P *et al* 2005 Dose verification of single shot gamma knife applications using VIPAR polymer gel and MRI 2005 *Phys. Med. Biol.* **50** 1235–50

Kavanagh B D and Timmerman R D 2006 Stereotactic radiosurgery and stereotactic body radiation therapy: an overview of technical considerations and clinical applications *Hematol. Oncol. Clin. North Am.* **20** 87–95

Kuo J S, Yu C, Petrovich A and Apuzzo M L 2003 The CyberKnife stereotactic radiosurgery system: description, installation and an initial evaluation of use and functionality *Neurosurgery* **53** 1235–9

Lightstone A W, Benedict S H, Bova F J, Solberg T D and Stern R L 2005 Intracranial stereotactic positioning systems: report of the American Association of Physicists in Medicine Radiation Therapy Committee Task Group No. 68 *Med. Phys.* **32** 2380–98

Mehta M P, Tsao M N, Whelan T J, Morris D E, Hayman J A, Flickinger J C, Millis M, Rogers C L and Souhami L 2005 The American society for therapeutic radiology and oncology (ASTRO) evidence-based review of the role of radiosurgery for brain metastases *Int. J. Radiat. Oncol. Biol. Phys.* **63** 37–46

Muacevic A, Staehler M, Drexler C, Wowra B, Reiser M and Tonn J-C 2006 Technical description, phantom accuracy, and clinical feasibility for fiducial free real-time image-guided spinal radiosurgery *J. Neurosurg. Spine* **5** 303–12

Murphy M J 2002 Fiducial-based targeting accuracy for external-beam radiotherapy *Med. Phys.* **29** 334–44

Murphy J M and Cox R S 1996 The accuracy of dose localization for an image-guided frameless radiosurgery system *Med. Phys.* **23** 2043–9

Nath R, Biggs P J, Bova F J, Ling C C, Purdy J A, Van de Geijn J and Weinhous M S 1994 AAPM code of practice for radiotherapy accelerators: report of AAPM Radiation Therapy Task Group No. 45 *Med. Phys.* **21** 1093–121

Nishizaki T *et al* 2006 The role of cyberknife radiosurgery/radiotherapy for brain metastases of multiple or large-size tumors *Minim. Invasive Neurosurg.* **49** 203–9

Pantelis E, Antypas C, Petrokokkinos L, Karaiskos P, Papagiannis P, Kozicki M, Georgiou E, Sakelliou L and Seimenis I 2008 Dosimetric characterization of CyberKnife radiosurgical photon beams using polymer gels *Med. Phys.* **35** 2312–20

Pappas E, Maris T G, Papadakis A, Zacharopoulou F, Damilakis I, Papanikolaou N and Gourtsogiannis N 2006 Experimental determination of the effect of detector size on profile measurements in narrow photon beams *Med. Phys.* **33** 3700–10

Pappas E, Petrokokkinos L, Angelopoulos A, Maris T G, Kozicki M, Dalezios I and Kouloulias V 2005 Relative output factor measurements of a 5 mm diameter radiosurgical photon beam using polymer gel dosimetry *Med. Phys.* **32** 1513–20

Romanelli P, Schaal D W and Adler J R 2006a Image-guided radiosurgical ablation of intra- and extra-cranial lesions *Technol. Cancer Res. Treat.* **5** 421–8

Romanelli P, Schweikard A, Schlaefer A and Adler J 2006b Computer aided robotic radiosurgery *Comput. Aided Surg.* **11** 161–74

Rossi R P, Lin P-J P, Rauch P L and Strauss K J 1985 Performance specifications and acceptance testing for x-ray generators and automatic exposure control devices *AAPM Report 14* (New York: American Association of Physicists in Medicine, American Institute of Physics)

Schell M C, Bova F J, Larson D A, Leavitt D D, Lutz W R, Podgorsak E B and Wu A 1995 Stereotactic radiosurgery *AAPM Report No. 54* (Madison, WI: Medical Physics Publishing)

Schweikard A, Shiomi H and Adler J 2004 Respiratory tracking in radiosurgery *Med. Phys.* **31** 2738–41

Shepard S J *et al* 2002 Quality control in diagnostic radiology *AAPM Report No. 74* (Madison, WI: Medical Physics Publishing)

Sorcini B and Tilikidis A 2006 Clinical application of image-guided radiotherapy, IGRT (on the Varian OBI platform) *Cancer Radiother.* **10** 252–7

Strassmann G, Braun I, Kress O, Richter D, Neidel H O, Klose K J, An H, Vogel B, Rose F and Engenhart-Cabillic R 2006 Accuracy of single-session extracranial radiotherapy for simple shaped lung tumor or metastasis using fast 3-D CT treatment planning *Int. J. Radiat. Oncol. Biol. Phys.* **66** 576–82

Tsao M N, Mehta M P, Whelan T J, Morris D E, Hayman J A, Flickinger J C, Millis M, Rogers C L and Souhami L 2005 The American society for therapeutic radiology and oncology (ASTRO) evidence-based review of the role of radiosurgery for malignant glioma *Int. J. Radiat. Oncol. Biol. Phys.* **63** 47–55

Wilcox E E and Daskalov G M 2007 Evaluation of Gafchromic® EBT film for CyberKnife® dosimetry *Med. Phys.* **34** 1967–74

Wu Q, Liang J and Yan D 2006 Application of dose compensation in image-guided radiotherapy of prostate cancer *Phys. Med. Biol.* **21** 1405–19

Wurm R and Okunieff P 2006 Intracranial and extracranial stereotactic radiosurgery and radiotherapy *Int. J. Radiat. Oncol. Biol. Phys.* **66** S1–S2

Yu C, Jozsef G, Apuzzo M L J and Petrovich Z 2004a Measurements of the relative output factors for CyberKnife collimators *Neurosurgery* **54** 157–62

Yu C, Main W, Taylor D, Kuduvalli G, Apuzzo M and Adler J R 2004b An anthropomorphic phantom study of the accuracy of CyberKnife spinal radiosurgery *Neurosurgery* **55** 1138–46